Towards Fault-Tolerant Computation: Simulation of a Hydrogen Molecule Using Logical Qubits

Yair Chizi,[1] Alexandru Cîrjaliu-Davidescu,[1] Antreas Ioannou,[1] and Santiago Sangro[1]
Delft University of Technology, Faculty of Applied Sciences, Minor Programme Quantum Science and Quantum Information

(Dated: 10 February 2025)

Corresponding to recent advancements in the scale and reliability of physical platforms, research on quantum computation and communication has placed greater emphasis on error-detection and fault-tolerance during computation under realistic conditions. Currently, fault tolerance is achieved by redundantly encoding a single 'logical' qubit over several physical qubits, thereby constructing a logical subspace of valid states sufficiently distanced to detect — and possibly correct — Z- and X-errors. In this paper, we aim to demonstrate the viability of logical coding in a simulation of a hydrogen molecule, exploring a simple 2 two-level logical encoding and Steane's logical qubits. The ground state and first excited state energies of the hydrogen molecule are calculated using Quantum Phase Estimation, with the molecular Hamiltonian encoded in a fault-tolerant logical framework. Our results show the potential of quantum chemistry simulations on fault-tolerance quantum computing, highlighting its viability even within the constraints of logical encoding.

I. INTRODUCTION & BACKGROUND

Quantum computing holds the promise of solving complex problems beyond the capabilities of classical computers, with applications spanning many fields such as cryptography[1], optimization[2], and chemistry[3,4]. Quantum computers possess the capability of improving quantum chemistry simulations which require an explicit representation of the wavefunction. Usually, quantum chemistry computations require very high accuracy in the results or have a high degree of entanglement in the system. While classical computers struggle to keep up with the exponential growth of dimension of the wave function, the inherent nature of quantum computers allows for higher accuracy and tractability of chemical simulations.

Multiple quantum algorithms have been invented that can already outperform classical ones[5]. In the field of chemistry, these include algorithms for approximating the ground-state energies of molecular systems[3]. One of these algorithms to approximate the ground-state energies implements the molecular Hamiltonian $\hat{H}$ as an evolution operator $U = e^{-i\hat{H}t}$. This is then used in addition to another technique known as Quantum Phase Estimation[6](QPE). In order to approximate the ground-state energy, the time evolution operator is used as the unitary gate and, given the ground state of the molecule, QPE is able to find the eigenphase corresponding to the ground state, which is directly related to its energy.

One of the major challenges in quantum computing is the presence of noise and errors during computation[7,8], posing a significant obstacle to producing results in noise-sensitive algorithms, especially in algorithms like QPE. Physical qubits, the fundamental information unit of a quantum computer, are prone to decoherence due to entanglement with the environment[9]. For this reason, the field of Quantum Error Correction (QEC) and fault-tolerant quantum computing have advanced rapidly over the past few decades. One approach to fault-tolerant quantum computation constructs a single *logical* qubit using multiple physical qubits, forming a subspace of the Hilbert space, known as the logical subspace, of valid code states. The degree of error protection that a particular logical representation offers is characterized by error distance, defined as the minimum number of error qubits required to transform one code state to another distinguishable state. In the context of quantum error-correcting codes, qubit error may be modeled by bit flips (Pauli X errors) and phase flips (Pauli Z errors)[10].

A variety of QEC codes have been developed to suit different computational needs. A repetition code is a simplistic implementation that encodes the logical basis states redundantly. More complex code schemes include CSS codes, such as Shor's code[11] or Steane's code[12], and topological codes, such as the surface code[10]. The diversity of QEC codes enables the tailored design of specialized architectures for specific circuits. QEC codes vary by qubit size overhead; types of detectable and correctable errors; and the existence[13], complexity, and degree of error protection of logical gates, limiting their suitability for specific problems. While these codes have been theoretically explored, active research is still being done on the implementation of such error correction codes on real hardware.

In this study, we combined quantum error-detecting codes with quantum chemistry simulations as a proof-of-concept to provide better insight into the feasibility and efficiency of simulating molecular systems on logical qubits. The hydrogen molecule (H_2) was chosen due to its inherent simplicity and known state energies[14], and the ground and first excited state energies for various bond lengths were obtained. This was done using two different kinds of logical qubit encodings: 2-qubit repetition code and Steane code. These logical qubits were used to encode the molecular Hamiltonian; however, the ancilla qubits of the Quantum Phase Estimation were represented by physical qubits due to physical limitations. The goal of this study is to evaluate and compare the resource requirements, computational precision, and error resilience of each logical encoding in the context of molecular simulations. By comparing physical and logical encoding results and utiliz-

ing metrics such as fidelity, we assess the robustness of these logical qubit architectures. We find that it is indeed possible to implement fault-tolerant quantum computation in quantum chemistry. We aim for this study to provide insights into implementing fault-tolerant quantum computation in quantum chemistry and to lay the groundwork for understanding resource scaling under realistic simulated conditions.

II. METHODOLOGY

A. Quantization and Representation of the Hamiltonian

To simulate chemistry systems on a quantum computer with the Schrodinger's equation, the Hamiltonian of the corresponding system needs to be represented in the framework of quantum computing. In order to do so, two steps are followed, as outlined in the work of Seeley et al.[15]. Firstly, the second-quantization is applied to the Hamiltonian in order to quantize it. Then, the Bravyi-Kitaev transformation[16] is applied, which allows us to represent the creation ($a^\dagger$) and annihilation (a) operators from the quantization formula in a quantum-computational form.

1. Second Quantization

In quantum computing, quantization is used in order to interpret molecular Hamiltonians. There are two main quantizations used in practice; first-quantization and second-quantization. In this study, we will make use of the second-quantization, due to limitations in terms of qubit simulation as well as time constraints. The second-quantization assumes that the two nuclei in the hydrogen molecule are fixed, and only the dynamics of the electrons are taken into account for the simulation[17]. This is known as the Born-Oppenheimer approximation (BOA)[18], and it allows us to derive the electronic Hamiltonian of the hydrogen molecule system:

$$H = \sum_{pq} h_{pq} a_p^\dagger a_q + \frac{1}{2} \sum_{pqsr} h_{pqsr} a_p^\dagger a_q^\dagger a_r a_s \tag{1}$$

2. Bravyi-Kitaev Transformation

The Bravyi-Kitaev (BK) transformation is a method for mapping fermionic operators, such as the creation ($a^\dagger$) and annihilation (a) operators, into qubit operators. This transformation is essential for quantum simulations of molecular systems, as it preserves the properties of fermionic wavefunctions while ensuring compatibility with quantum computation frameworks[16].

A key advantage of the Bravyi-Kitaev transformation is its computational efficiency. While representing a fermionic operator typically requires $O(n)$ qubit operations for a system with n fermionic modes, the BK transformation reduces this to $O(logn)$ qubit operations[15]. This efficiency is achieved by encoding both the occupation number and parity information hierarchically across qubits.

The hierarchical encoding in the BK transformation provides significant computational advantages. By requiring only $O(\log n)$ operations per fermionic operator, the transformation optimizes the representation of molecular Hamiltonians on quantum computers. This efficiency is crucial for scalable simulations of molecular systems[16].

In this study, we applied the BK transformation to represent the second-quantized Hamiltonian of the hydrogen molecule in the qubit computational framework. The resulting Hamiltonian, expressed in terms of Pauli operators, is given by:

$$\begin{aligned}\hat{H} = {} & \omega_1 \sigma^I + \omega_2 \sigma_0^z + \omega_3 \sigma_1^z + \omega_4 \sigma_2^z + \omega_5 \sigma_0^z \sigma_1^z \\ & + \omega_6 \sigma_0^z \sigma_2^z + \omega_7 \sigma_1^z \sigma_3^z + \omega_8 \sigma_0^x \sigma_1^z \sigma_2^x + \omega_9 \sigma_0^y \sigma_1^z \sigma_2^y \\ & + \omega_{10} \sigma_0^z \sigma_1^z \sigma_2^z + \omega_{11} \sigma_0^z \sigma_2^z \sigma_3^z + \omega_{12} \sigma_1^z \sigma_2^z \sigma_3^z \\ & + \omega_{13} \sigma_0^x \sigma_1^z \sigma_2^x \sigma_3^z + \omega_{14} \sigma_0^y \sigma_1^z \sigma_2^y \sigma_3^z + \omega_{15} \sigma_0^z \sigma_1^z \sigma_2^z \sigma_3^z. \end{aligned} \tag{2}$$

The coefficients $(\omega_1, \omega_2, \ldots)$ for the molecular Hamiltonian were derived from the one-body and two-body h coefficients obtained using the `StatevectorSimulator` package from Qiskit and then calculated based on a standard methodology outlined in the work of Z. Zhang[19].

B. Eigenenergy Measurement via Quantum Phase Estimation

Quantum Phase Estimation (QPE), is a foundational quantum algorithm used to determine the eigenvalues of a given unitary operator. In quantum chemistry, this method is particularly valuable because the eigenvalues of molecular Hamiltonians correspond to the energy levels of molecules, which are critical for understanding chemical properties and reactions[20]. This section discusses the theoretical basis of QPE, its significance in this study, and its application to simulate the hydrogen molecule.

1. Theoretical Framework

Given a unitary operator U and an eigenstate $|\psi\rangle$, the QPE algorithm estimates the eigenvalue $e^{2\pi i\phi}$, where ϕ is the associated phase. The algorithm works by encoding the phase ϕ of the eigenvalue into the quantum state of ancilla qubits. The quantum system begins with ancilla qubits in a superposition state and target qubits in an eigenstate of the unitary operator. Controlled applications of the operator U allow the phase ϕ to accumulate on the ancilla qubits. Finally, the inverse Quantum Fourier Transform (QFT) is applied to the ancilla qubits to extract the phase in binary form. The precision of QPE increases with the number of ancilla qubits, allowing for accurate determination of the phase and its associated eigenvalue[7].

2. Relevance to Quantum Chemistry

QPE is an essential algorithm for quantum chemistry because it enables the determination of molecular energy eigenvalues, which are fundamental for predicting chemical phenomena. In this project, QPE was chosen to estimate the ground state energy and first excited state energy of the hydrogen molecule. The deterministic nature of QPE and its ability to achieve high precision make it a suitable approach for simulating molecular systems. Furthermore, QPE's compatibility with the Bravyi-Kitaev transformation allows efficient representation of fermionic Hamiltonians on a quantum computer. This ensures that the molecular properties are accurately captured during simulation[4].

3. Implementation

The molecular Hamiltonian of the hydrogen molecule was first represented in the second-quantized form and mapped into the qubit framework using the Bravyi-Kitaev transformation. The resulting qubit Hamiltonian was used to construct the unitary operator

$$U = e^{-iHt}, \tag{3}$$

where H is the Hamiltonian, and t is the time of evolution. A parameterized quantum circuit (further discussed in section II C 2) was designed to simulate this unitary operator, with the parameters derived from the Hamiltonian coefficients.

To perform Quantum Phase Estimation (QPE), the initial state was prepared to ensure significant overlap with the ground state of the Hamiltonian. The initial state was calculated using an exact eigensolver of the Hamiltonian provided. The QPE circuit consisted of six ancilla qubits and four target qubits. The ancilla qubits encoded the phase information through controlled applications of the unitary operator, while the target qubits represented the molecular Hamiltonian. An inverse Quantum Fourier Transform was applied to the ancilla qubits to extract the binary representation of the phase.

The resulting binary phase measurement was converted into the ground-state energy using the relationship

$$E = -\frac{\phi \cdot 2\pi}{t}, \tag{4}$$

where ϕ is the phase and t is the evolution time. This approach enabled high-precision estimation of the hydrogen molecule's ground-state energy. The energy was used to validate the accuracy of the quantum simulation.

C. Quantum Circuit for the Hydrogen Molecule Hamiltonian

Having encoded the molecular Hamiltonian in the quantum computational framework, we proceeded to construct the quantum circuit for simulating the hydrogen molecule. Following the methodology outlined by Z. Zhang[19], a two-phase approach was implemented for circuit design. The first phase involved the Trotterization of the time evolution operator, e^{-iHt}, using a Suzuki-Trotter approximation[21]. In the second phase, individual quantum circuits were constructed for each operator in the Hamiltonian. These circuits were then combined to implement the full-time evolution operator, enabling precise simulation of the hydrogen molecule's dynamics.

1. Trotterisation

For the simulation, the time evolution operator e^{-iHt} was approximated using a fourth-order Suzuki-Trotter expansion[21]. This refinement improved upon Zhang's original approach, which employed a first-order approximation. The fourth-order expansion effectively reduces the Trotter error compared to the first-order approximation.

The circuit was initially designed using the first-order Suzuki-Trotter decomposition, given by:

$$e^{-iHt} \approx \prod_{k=1}^{15} e^{-iH_k t}, \tag{5}$$

where $H = \sum_{k=1}^{15} H_k$ and the Hamiltonian H is split into 15 non-commuting terms $H_1, H_2, \ldots, H_{15}$.

The modular nature of the circuit design allowed the time evolution operator to be divided into smaller time steps, enabling the reuse of each subcircuit. This modularity facilitated the implementation of the fourth order Suzuki-Trotter decomposition. However, when encoding the simulation into logical qubits, the first-order approximation was deliberately retained to reduce the number of operations required and thereby minimize the circuit depth.

2. Circuit Composition

With the evolution operator approximated, the quantum circuit was created using a straightforward approach. The method used the fact that the time evolution operator could be expressed as a product of exponential functions of the form $e^{-iH_i t}$. Each exponential function was individually encoded into a quantum circuit, and these circuits were then sequentially appended to construct the full quantum circuit.

To encode each exponential function into a circuit, a Taylor series expansion[22] given by:

$$e^A = \sigma^I + A + \frac{A^2}{2!} + \frac{A^3}{3!} + \cdots = \sum_n \frac{A^n}{n!}, \tag{6}$$

was employed for the operators. The Taylor expansion allowed the exponential operators to be expressed as a series,

revealing trigonometric patterns such as cosine and sine functions. For example, the operator $e^{-i\theta\sigma_0^z}$ was expanded as:

$$\begin{aligned} e^{-i\theta\sigma_0^z} &= \sigma I + (-i\theta\sigma_0^z) + \frac{(-i\theta\sigma_0^z)^2}{2!} + \frac{(-i\theta\sigma_0^z)^3}{3!} + \frac{(-i\theta\sigma_0^z)^4}{4!} + \cdots \\ &= \sigma^I - i\theta\sigma_0^z - \frac{\theta^2}{2!}\sigma^I + \frac{i\theta^3}{3!}\sigma_0^z + \frac{\theta^4}{4!}\sigma^I - \cdots \\ &= \left(1 - \frac{\theta^2}{2!} + \frac{\theta^4}{4!} - \cdots\right)\sigma^I + i\left(\theta - \frac{\theta^3}{3!} + \frac{\theta^5}{5!} + \cdots\right)\sigma_0^z \\ &= \cos(\theta)\sigma^I - i\sin(\theta)\sigma_0^z \\ &= \begin{bmatrix} \cos(\theta) - i\sin(\theta) & 0 \\ 0 & \cos(\theta) + i\sin(\theta) \end{bmatrix} \\ &= \begin{bmatrix} e^{-i\theta} & 0 \\ 0 & e^{i\theta} \end{bmatrix}, \end{aligned} \tag{7}$$

where $\theta = \omega \cdot t$. This equation was taken from the work of Z. Zhang[19].

A similar approach was followed for the rest of the Hamiltonian's terms, creating a matrix for each. This matrix representation was then mapped to quantum gates, allowing efficient implementation in the quantum circuit. The modularity of the approach ensured that each exponential term could be independently encoded into a subcircuit. By sequentially appending these subcircuits, the overall circuit faithfully approximated the desired time evolution operator.

D. Logical Qubit Design

A major challenge in quantum computing is the presence of noise and errors that arise during computation[7,8]. In particular, the Hamiltonian for the hydrogen molecule is highly susceptible to qubit error due to the large amount of gates, the high degree of qubit entanglement, and high qubit wait times. The presence and accumulation of errors can significantly disturb the qubit state, and lead to inaccurate and undesirable simulation results. Addressing this issue, we implement an error-detecting code and an error-correcting code to enhance the reliability of the quantum circuit.

In this paper, the implementation of a specific code consists of the implementation of tailored logical gates necessary for the Hamiltonian circuit. This approach allows for the substitution of the physical gates in the original Hamiltonian with their logical counterparts, which is consistent with scalable proposals of QEC circuits in literature[23,24]. The effectiveness of logical gates is evaluated by their logical safety and transversality. Logically safe gates are gates that transform a valid logical state to another. Transverse logical gates do not entangle physical qubits within the same logical unit[25,26]. In particular, transversality is a desired characteristic of logical gates as it prevents an error on one physical qubit from propagating across the logical qubit.

Notwithstanding design considerations, complex codes inherently impose practical constraints that limit their utility. Complex codes may greatly augment the qubit register size, the total number of gates, and the complexity of a circuit, and may possibly introduce non-unitary operations such as measurements. Consequently, embedding logical codes inevitably demands greater compute power and longer execution times[27], possibly exceeding the capabilities of currently available quantum systems, either due to system timeouts, insufficient qubit register size, or high error rates.

As such, in this section, we proceed to examine and implement two logical codes for the hydrogen molecule Hamiltonian. For each logical code, we introduce implementations for relevant logical gates and evaluate their effectiveness. Section II D 1 offers a simplistic error-detecting 2-qubit repetition code. In contrast, section II D 2 explores an implementation of the error-correcting Steane code. Finally, section II D 3 introduces methodologies for evaluating the logical implementations of the Hamiltonian.

1. 2-Qubit Repetition Code

The 2-Qubit Repetition Code is a simplistic error-detection code in quantum computing. For the limited qubit overhead, the code offers the ability to detect a single qubit error; in this implementation, a single bit-flip (Pauli X errors) may be detected. Notably, the limitation of a single qubit error is not limited to one physical qubit, but rather to the entire logical qubit as a whole. Moreover, phase-flips (Pauli Z errors) remain undetectable.

Valid logical states for a single qubit are necessarily a superposition of the logical computational basis, $|\psi\rangle_L = \alpha|0\rangle_L + \beta|1\rangle_L$, whereby $|0\rangle_L = |00\rangle$ and $|1\rangle_L = |11\rangle$. Alternatively, the logical subspace may be defined by the stabilizer group $S_{2-\text{Qubit}} = \langle II, ZZ\rangle$ that fixes only the logical subspace in the entire Hilbert space.

The encoder circuit for multiple qubits is shown in Fig. 1. The encoder operates by passing the desired state through the first physical qubit and performing an entanglement CNOT gate targeted at the second physical qubit, initially at ground. The entanglement operation results in a superposition of states of even parity, which are valid logical states. The encoder may be extended for multiple qubits by applying the aforementioned encoder circuit for physical qubit pairs.

The implementations for the logical gates relevant for the Hamiltonian are provided in Table I in Appendix A. As presented, all logical gates are logically safe, and thus always transform a valid logical state to another. In particular, the parametrized rotation gates are logically safe even under float-point errors.

Moreover, as exhibited in Table I, barring the Hadamard and parametrized rotation gates, all logical gates are implemented transversally. Such gates are protected to the extent that an error occurring in one physical qubit does not influence other physical qubits within the same logical unit,

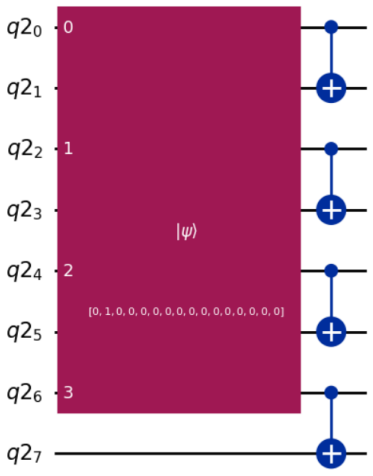

FIG. 1. Initializing a logical qubit using the 2-qubit repetition code. A CNOT (CX) gate entangles the original qubit with an auxiliary qubit initialized to $|0\rangle$. The box represents the initial quantum state $|\psi\rangle$, displaying its amplitude components in the computational basis.

and thereby could be detected. Consistent with the Eastin-Knill theorem[25], since the CNOT and parametrized phase gates are implemented transversally, the Hadamard gate (See Fig. 2) may not be implemented transversally to form a transverse universal set of quantum operators. Similarly, the parametrized rotation gates must also not be transverse. In comparison to the transverse gates, the non-transverse are not fault-tolerant. For instance, in the logical Hadamard, a bit-flip on the first physical qubit following the Hadamard gate produces an erroneous yet valid logical state, which is never detectable.

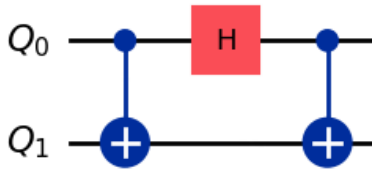

FIG. 2. The physical non-transverse implementation of the logical Hadamard for the 2-qubit code.

This encoding is a very simple quantum error detection code, but it has significant limitations. The 2-qubit repetition code cannot correct errors, nor detect errors that affect both qubits simultaneously or other common errors such as phase-flip errors (Z errors). The 2-qubit repetition code is also inefficient, as it doubles the number of physical qubits while offering minimal error-handling capabilities. In contrast, more advanced correction codes provide better detection and correction for marginally more qubit overhead.

As such, for more circuit-intensive qubits, for which precision and correction are more valuable, we opt to employ more complex, yet more resource-demanding, logical codes to ensure minimization of errors.

2. *Steane Code*

The Steane code [[7,1,3]][28] is a Calderbank-Shor-Steane (CSS) code that encodes a single logical qubit using seven physical qubits. Being a 3-distance code, the Steane allows for the reliable detection of up to two qubit errors (any Pauli error), and the reliable correction of one error. Similarly to the previous code, a valid logical state may be represented by the superposition of the logical basis states $|\psi\rangle_L = \alpha|0\rangle_L + \beta|1\rangle_L$, where the logical basis states are given in Eq. 8 and Eq. 9.

$$\begin{aligned}|0\rangle_L \;=\; \tfrac{1}{\sqrt{8}}\;&(|0000000\rangle + |1010101\rangle + |0110011\rangle \\ &+\; |1101100\rangle + |0001111\rangle + |1011010\rangle \\ &+\; |0111100\rangle + |1101001\rangle)\end{aligned} \tag{8}$$

$$\begin{aligned}|1\rangle_L \;=\; \tfrac{1}{\sqrt{8}}\;&(|1111111\rangle + |0101010\rangle + |1001100\rangle \\ &+\; |0010011\rangle + |1110000\rangle + |0100101\rangle \\ &+\; |1000011\rangle + |0010110\rangle)\end{aligned} \tag{9}$$

Similarly to the 2-qubit repetition code, the encoder circuit for the Steane code may be constructed using an encoder for a single qubit. The encoder circuit for a single logical qubit[29], where the desired state is passed through the first physical qubit, is exhibited in Fig. 3. Notably, since the resultant state is highly entangled, the encoder circuit may not be able to effectively protect against qubit errors and likely result in an invalid uncorrectable state.

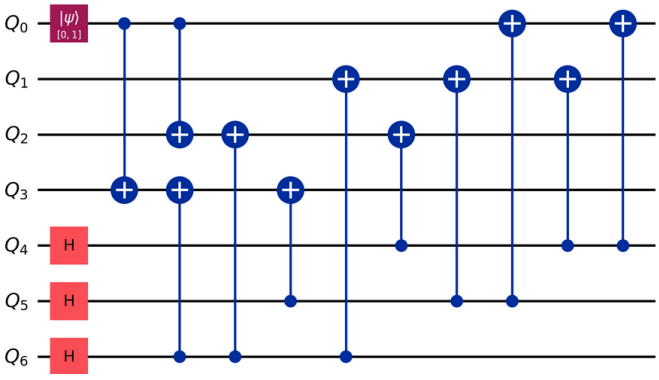

FIG. 3. Initializing a logical qubit in the Steane code using a single-qubit encoder[29]. The desired qubit state $|\Psi\rangle$ is passed through the first logical qubit.

The implementations of the logical gates relevant for the Hamiltonian are provided in Table II in Appendix A. The structure of the physical state of the computational basis states allows for the expedient transversal implementation for the Pauli X_L and Z_L gates, with $X_L = \bigotimes_{k=1}^{7} X_k$ and $Z_L = \bigotimes_{k=1}^{7} Z_k$. Likewise, the Hadamard gate may be implemented transversally,$H_L = \bigotimes_{k=1}^{7} H_k$. Notably, this pattern does not

extend for the logical Y gate, although it remains transversal as demonstrated in Eq. 10.

$$\begin{aligned} Y_L &= iX_LZ_L \\ &= X_7Z_7X_6Z_6\bigotimes_{k=1}^{5} iX_kZ_k \\ &= X_7Z_7X_6Z_6\bigotimes_{k=1}^{5} Y_k \end{aligned} \tag{10}$$

While requiring additional derivation, the logical CNOT gate may also be implemented transversely, with $\mathrm{CX}_L = \bigotimes_{k=1}^{7} C_kX_k$, where C_iX_j refers to applying a CNOT gate on the i-th physical qubit of the logical control and the j-th physical qubit of the logical target. Under this implementation, the transverse logical CNOT transforms a state $|c,t\rangle$ into the state $|c,c\oplus t\rangle$, where $\oplus$ operator is the bit-wise exclusive or operator applied over the physical bits encoding the logical one. To demonstrate the correctness, we can observe that any computational Z-basis state, $|\Psi_7^{\text{even}}\rangle$ comprising $|0\rangle_L$ fixes the logical basis states under CNOT (Eq. 11). On the contrary, any computational Z-basis state,$|\Psi_7^{\text{odd}}\rangle$, comprising $|1\rangle_L$ causes the computational state to alternate (Eq. 12). Hence, the superposition $|0\rangle_L$ fixes both $|0\rangle$ and $|1\rangle$ under CNOT, while $|1\rangle_L$ causes the basis states to alternate as expected.

$$\begin{aligned} |\Psi_7^{\text{even}},\Psi_7^{\text{even}}\oplus 0_L\rangle &= |\Psi_7^{\text{even}},0_L\rangle \\ |\Psi_7^{\text{even}},\Psi_7^{\text{even}}\oplus 1_L\rangle &= |\Psi_7^{\text{even}},1_L\rangle \end{aligned} \tag{11}$$

$$\begin{aligned} |\Psi_7^{\text{odd}},\Psi_7^{\text{odd}}\oplus 1_L\rangle &= |\Psi_7^{\text{odd}},0_L\rangle \\ |\Psi_7^{\text{odd}},\Psi_7^{\text{odd}}\oplus 0_L\rangle &= |\Psi_7^{\text{odd}},1_L\rangle \end{aligned} \tag{12}$$

Similar to the CNOT gate, the controlled Z gate can also be implemented transversely such that $\mathrm{CZ}_L = \bigotimes_{k=1}^{7} C_kZ_k$. The implementation may be demonstrated by considering $CZ_k = H_kCX_kH_k$.

Despite the transversality of the previously mentioned gates, the implementation for the parametrized rotation gates is not only non-transversal but also non-trivial. Firstly, provided an implementation for $R_z(\theta)_L$, $R_x(\theta)_L$ may be constructed such that $R_x(\theta)_L = H_LR_z(\theta)_LH_L$. In this paper, we have chosen a measurement-based implementation for $R_z(\theta)$ that uses magic-state injection[13] (Fig. 4). Notably, the rotation gates in the Hamiltonian circuit require a variable, float-point parametrization, preventing an approximation-based implementation. The magic-state injection produces the desired rotation in four steps. First, the implementation initializes an ancilla that holds the desired rotation. Second, the ancilla entangles with the targeted logical qubit so that the expected logical state is entangled with $|0\rangle_L$, and a similar logical state is entangled with $|1\rangle_L$ (See Eq. 13). Third, the ancilla is measured in the Z-basis to collapse the state to one of two outcomes. Finally, if the ancilla is measured to be $|1\rangle_A$, i.e. the logical state is not the expected state, then the logical qubit may be corrected.

$$\begin{aligned} |\Psi\rangle_L|0\rangle_A &\rightarrow |\Psi\rangle\left(e^{-i\pi/2}|0\rangle_A + e^{\pi/2}|1\rangle_A\right) \\ &\rightarrow \left(\alpha e^{-i\pi/2}|0\rangle_L + \beta e^{\pi/2}|1\rangle_L\right)|0\rangle_A \\ &\quad + \left(\alpha e^{i\pi/2}|0\rangle_L + \beta e^{-\pi/2}|1\rangle_L\right)|1\rangle_A \end{aligned} \tag{13}$$

Magic-state injection, while allowing for a correct computation of the Rz gate, constrains its utility in relation to the circuit as a whole. The inclusion of the measurement operation prevents the conversion of the Hamiltonian into a controlled operator, which the QPE circuit is heavily reliant on. Moreover, the inclusion of the ancilla further increases the qubit register size. Finally, the ancilla qubit must interact with every qubit, thereby impeding the computation and causing a long idle time for the target qubits.

Moreover, the magic-state injection implementation is heavily entangled with the target qubit, which may allow errors to propagate throughout the logical qubit. Notably, the ancilla qubit may be substituted with a logical ancilla to avoid over-entangling a single qubit. Encoding the ancilla through Steane code will improve the parallelization of the circuit.

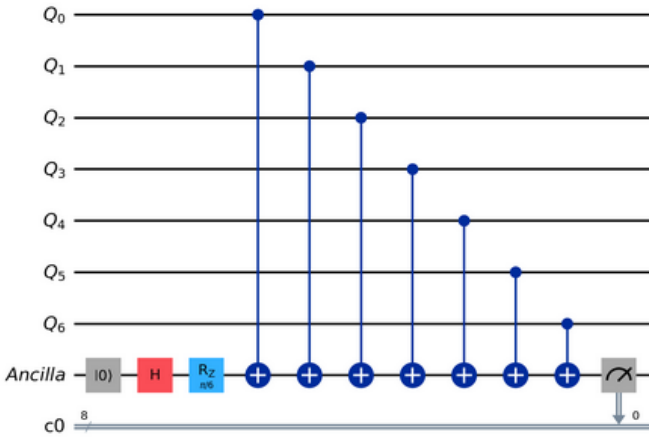

FIG. 4. Measurement-based implementation for the Rz gate using magic-state injection. The ancilla holds the transformation. The state correction circuit is omitted.

3. *Simulation of Fidelity and Error Detection*

In examining the efficacy of the logical qubits, we implemented a simulation of the Hamiltonian circuit under noise conditions. To introduce noise, we have added a noise model to the circuit that inserts a Pauli error gate at a location[23] in the circuit with error probability per gate p. Individually, the Pauli gates have a $\frac{p}{3}$ of affecting a gate. The resulting noisy state, $|S_{\text{noisy}}\rangle$, extracted from the simulation is compared to the ideal state, $|S_{\text{ideal}}\rangle$, by computing its fidelity.

$$F(S_{\text{noisy}},S_{\text{ideal}}) = |\langle S_{\text{noisy}}|S_{\text{ideal}}\rangle|^2 \tag{14}$$

The error detection capability is measured by identifying invalid states following the final measurement of the Hamiltonian to compute an observed error rate, r_{actual}. While this approach to error detection measurement will not identify every detectable error, it will, nonetheless, provide a lower bound for the error rate. The expected error rate, r_{expected}, can be

modeled using a binomial distribution.

$$r_{\text{expected}} = 1 - (1-p)^{\#\text{physical gates}} \tag{15}$$

III. RESULTS

In order to test the accuracy of the Quantum Phase Estimation as well as the Hamiltonian circuit derived, we calculated the ground state and the first excited state energies at different bond lengths of the Hydrogen molecule. Furthermore, these results were compared to previous studies, as well as to the results obtained using Qiskit's Variational Quantum Eigensolver. The simulation makes use of the Quantum Phase Estimation with six ancillary qubits. Furthermore, the 2-Qubit Repetition Code was implemented on the Hamiltonian circuit and tested for fidelity and detected error rate. Due to hardware limitations, the Steane code could not have been extensively and reliably tested and was summarily omitted in the results. The corresponding code can be found in our GitHub repository.

A. Ground State Energies

The ground state energy was calculated at 17 different bond lengths, to match Kolos's and Wolniewicz's results[14]. The results obtained are presented in Fig. 5. It is important to note that this simulation did not calculate nuclear repulsion energy directly but included it in the final results for comparison purposes. Comparing the ground state energies at different bond lengths we can observe that the energy curves follow a similar trend. Due to the use of Quantum Phase Estimation and hardware limitations, the use of six ancillary qubits limits the precision of our results. Still, the overall shape seems to be in line with Kolos's and Wolniewicz's results. The shift between energy curves is likely due to the use of slightly different methods when calculating the Hamiltonian.

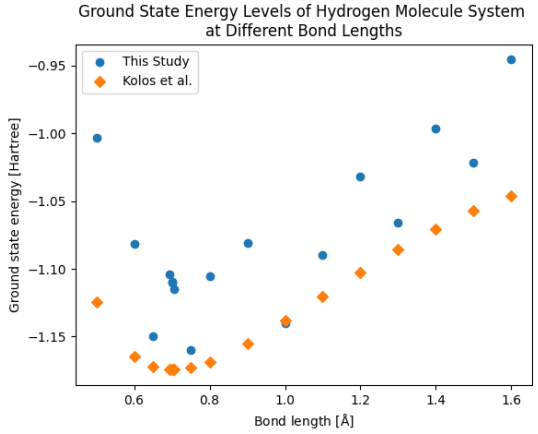

FIG. 5. Ground state energy curves from this study and Kolos's and Wolniewicz's study[14]. The x-axis represents the ground state energy in Hartrees. The y-axis shows the different distances between the nuclei of the two hydrogen atoms in Armstrongs. Both studies follow a comparable curve; however, the precision of this study is inherently limited by the use of six ancillary qubits for QPE.

The bond length with the lowest ground state energy differs for both studies; 0.65 Å for this study, and 0.701 Å for Kolos's and Wolniewicz's study. Additionally, the lowest ground state energy in this study is found to be -1.1493766 Hartrees. Kolos's and Wolniewicz's lowest ground state energy corresponds to -1.17447482 Hartrees. The absolute difference between them is 0.025 Hartrees. Despite these differences, the deviations in both energy values and bond lengths are relatively small, indicating that QPE provides results that align well with established methods.

To quantify the accuracy of our simulation, we calculated the mean absolute difference of the ground state energies, as well as the error percentage. We obtained a mean absolute difference value of 0.05710491 Hartrees, and an error percentage of 5.057%. These findings suggest that, even with a limited number of ancillary qubits, Quantum Phase Estimation can reliably approximate the ground state energy of a molecular system.

B. First Excited State Energies

The first excited state energies were calculated using the same procedure described in Section III A. However, the results obtained in this study were compared to the energies calculated using Qiskit's Variational Quantum Eigensolver (VQE). Fig. 6 shows the first excited state energies for both methods.

Both energy curves follow the same decreasing trend. Despite the limited precision of QPE, the results match the overall shape of the energy curve calculated through Qiskit's VQE fairly accurately. The bond length with the lowest ground state energy is the same for both methods; 1.6 Å . Furthermore, the lowest ground state energy in this study is found to be -0.94553626 Hartrees. Qiskit's VQE lowest ground state energy corresponds to -0.90191182 Hartrees. The absolute difference between them is 0.0436 Hartrees. The deviation in the lowest energy value is fairly small. Quantum Phase Estimation seems to perform accurately for both the ground state and the first excited state. Finally, the mean absolute difference and percentage error were calculated. We obtained a mean absolute difference value of 0.01678013 Hartrees and an error percentage of 2.860%.

To conclude, the simulation using Quantum Phase Estimation with six ancillary qubits successfully reproduced the overall general trend of ground state and first excited state energy curves for the hydrogen molecule, aligning closely with Kolos and Wolniewicz's results, as well as Qiskit's VQE. Despite small deviations, the findings demonstrate the feasibility

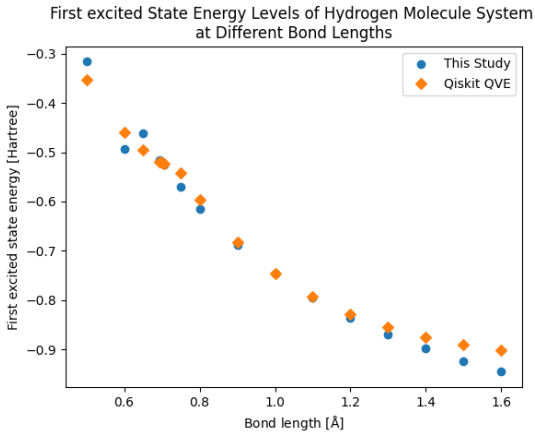

FIG. 6. First excited state energy curves obtained using this study's logical qubits and Qiskit's VQE. The x-axis represents the ground state energy in Hartrees. The y-axis shows the different distances between the nuclei of the two hydrogen atoms in Armstrongs. Both methods follow a comparable trend; however, the accuracy of the logical qubit approach is inherently limited by the use of six ancillary qubits for QPE.

of using logical qubits in order to reproduce molecular simulations.

C. Fidelity and Error Detection

To evaluate the suitability of the logical codes when applied on the Hamiltonian circuit, the fidelity and error detection rate were calculated for the single-qubit encoding and the 2-qubit repetition logical encoding. The Steane logical encoding could not have been tested repeatedly in a local simulation due to its large qubit register and gate complexity. As the error probability is applied per gate, the effects of the error probability, p, were investigated for small values $0 \leq p \leq 0.1$. For every gate error probability, the fidelity and error rate were calculated on $N_{\text{noise model}} = 100$ noisy Hamiltonian circuits, which were modified by the noise model as defined in Section II D 3. For error detection, $N_{shots} = 100$ shots were simulated for every noisy Hamiltonian circuit.

The average fidelity of the hydrogen Hamiltonian is presented in Fig. 7. The average fidelity appears to correlate negatively with the error probability, consistent with the lack of error correction mechanisms. The Hamiltonian's computed state appears to become unreliable ($F = 0.8$) at a low gate error probability $p_{0.8} \sim 0.02$. The 2-qubit repetition code appears to perform worse than the single qubit, with a margin that positively correlates with the gate error probability, consistent with the heightened circuit complexity and increased gate count. Nonetheless, at a low error probability ($p < 0.02$), the fidelity of the two encodings is comparable.

The post-measurement error rate for the 2-qubit logical encoding is presented in Fig. 8. Compared to the expected error rate (see Section II D 3), the encoding appears to detect $r_{\text{actual}}/r_{\text{expected}} \sim 66\%$ of expected errors. As the noise model considers only Pauli errors, this finding is consistent with the inability of the 2-qubit logical code to detect phase-flip errors or any error that was transformed into a phase-flip error by the circuit.

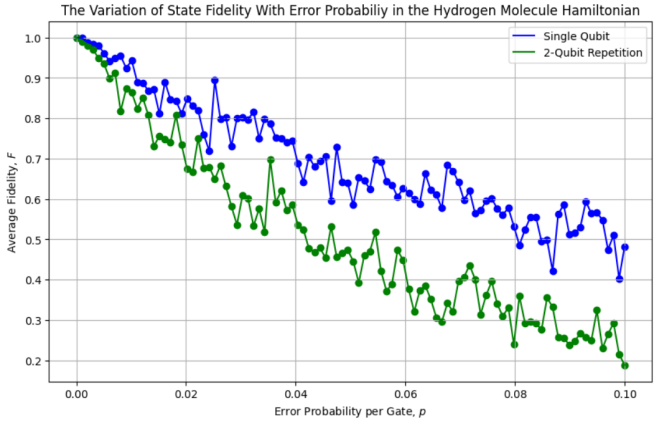

FIG. 7. The state fidelity of the 1-qubit encoding and the 2-qubit encoding for the Hydrogen Molecule Hamiltonian in variation of the gate error probability, p, within one standard deviation. ($N = N_{\text{Noise Model}} = 100$ samples per error probability).

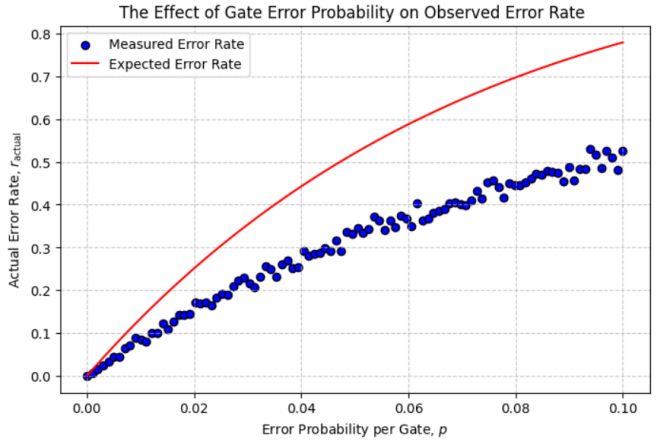

FIG. 8. The observed error rate for the 2-qubit logical code, r_{actual} in variation of the gate error probability p. The expected error rate, r_{expected}, for the noise model is included. ($N = N_{\text{Noise Model}} \cdot N_{\text{shots}} = 10^4$ samples per error probability).

IV. DISCUSSION & CONCLUSION

This study aimed to show how to approximate the ground state energy and first excited state energy of the hydrogen molecule at different bond lengths using Quantum Phase Estimation on logical qubits. A qualitative and quantitative analysis of the simulation results was performed. Due to hardware limitations, we made use of six ancilla qubits,

and only the molecular Hamiltonian was encoded in a fault-tolerant logical framework. The ancilla qubits of the QPE were mapped to physical qubits. Despite these limitations, our results show that the energies of the system can be fairly well approximated, highlighting the viability of reducing the noise when solving molecular systems through quantum phase estimation.

The study faced many limitations, mainly due to the developing state of quantum computing and the demanding complexity of the circuit. Notably, only the double-qubit logical framework was used to encode the Hamiltonian, and this implementation lacked error correction. While the purpose of the study was to provide further proof of the viability of using QPE to solve molecular systems, its practical application to larger molecular systems remains challenging. The current hardware limitations, including the small number of qubits and high error rate, make it infeasible to solve molecular systems which are computationally intractable for classical computers. Furthermore, even classical simulations of quantum circuits cannot deal with the computational cost when increasing the molecular system significantly. Until the field of quantum computing is more advanced, the use of QPE for large molecular systems will most likely remain theoretical.

One of the key observations from our study is that, despite current limitations, the Quantum Phase Estimation (QPE) method remains a promising approach for molecular energy calculations. Therefore, this study could be expanded to other error-correcting codes. Furthermore, through alternative approximation methods[30], the hydrogen molecule could be encoded with fewer qubits, making it more feasible to implement on real hardware and obtain more practical results. Finally, there is still limited research on the optimal logical encoding to simulate molecular systems. Future work could build on our study as a benchmark, exploring alternative encoding methods to determine the most effective approach for quantum chemistry simulations.

Appendix A: Gate Designs for Logical Encodings

This appendix provides the gate designs for the logical encodings used in the fault-tolerant quantum computation framework. The first table (Table I) describes the 2-Qubit Repetition Encoding, while the second table (Table II) details the Steane/[[7,1,3]] Code.

Name	Symbol	Design Formula	Safe	Transverse
Hadamard	$H_L(Q)$	$CX(Q^1,Q^2)\ H(Q^1)\ CX(Q^1,Q^2)$	Yes	No
Pauli X	$X_L(Q)$	$X(Q^1)\ X(Q^2)$	Yes	Yes
Pauli Y	$Y_L(Q)$	$Y(Q^1)\ X(Q^2)$	Yes	Yes
Pauli Z	$Z_L(Q)$	$Z(Q^1)$	Yes	Yes
CX	$CX_L(Q_1,Q_2)$	$CX({Q_1}^1,{Q_2}^1),CX({Q_1}^2,{Q_2}^2)$	Yes	Yes
CY	$CY_L(Q_1,Q_2)$	$CY({Q_1}^1,{Q_2}^1),\ CX({Q_1}^2,{Q_2}^2)$	Yes	Yes
CZ	$CZ_L(Q_1,Q_2)$	$CZ({Q_1}^1,{Q_2}^1)$	Yes	Yes
Rotation	${R^X}_L(Q)$	$CX(Q^1,Q^2)\ R^X(Q^1)\ CX(Q^1,Q^2)$	Yes	No
Phase	$P_L(Q)$	$P(Q^1)$	Yes	Yes
CPhase	$CP_L(Q_1,Q_2)$	$CP({Q_1}^1,{Q_2}^1)$	Yes	Yes
Global Ph	$Ph_L(Q,\theta)$	$I(Q^1)\cdot e^{-\theta i}$	Yes	Yes

TABLE I. Gate Design for the 2-Qubit Repetition Encoding. Safety refers to logical safety. ${Q_X}^Y$ represents the Y^{th} physical qubit in logical qubit Q_X.

Gate	Symbol	Design Formula	Safe	Transverse
Hadamard	$H_L(Q)$	$\bigotimes k = 1^7 H(Q^k)$	Yes	Yes
Pauli X	$X_L(Q)$	$\bigotimes k = 1^7 X(Q^k)$	Yes	Yes
Pauli Y	$Y_L(Q)$	$\bigotimes k = 6^7 X(Q^k) Z(Q^k) \bigotimes k = 1^5 Y(Q^k)$	Yes	Yes
Pauli Z	$Z_L(Q)$	$\bigotimes k = 1^7 Z(Q^k)$	Yes	Yes
CX	$CX_L(Q_1,Q_2)$	$\bigotimes k = 1^7 CX(Q_1^k, Q_2^k)$	Yes	Yes
CZ	$CZ_L(Q_1,Q_2)$	$\bigotimes k = 1^7 CZ(Q_1^k, Q_2^k)$	Yes	Yes
Rotation	${R^{X,Z}}_L(Q)$	See Section II D 2	Yes	No
Global Ph	$Ph_L(Q)$	$I(Q^1)$	Yes	Yes

TABLE II. Gate Design for the Steane code [[7,1,3]]. The table contains only the relevant gates for the implementation of the hydrogen molecule Hamiltonian. The implementation for the rotation is demonstrated in section II D 2. ${Q_X}^Y$ represents the Y^{th} physical qubit in logical qubit Q_X.

[1] C. H. Bennett and G. Brassard, "Quantum cryptography: Public key distribution and coin tossing," Theoretical computer science **560**, 7–11 (2014).
[2] E. Farhi, J. Goldstone, and S. Gutmann, "A quantum approximate optimization algorithm," arXiv preprint arXiv:1411.4028 (2014).
[3] A. Aspuru-Guzik, A. D. Dutoi, P. J. Love, and M. Head-Gordon, "Simulated quantum computation of molecular energies," Science **309**, 1704–1707 (2005).
[4] Y. Cao, J. Romero, J. P. Olson, M. Degroote, P. D. Johnson, M. Kieferová, I. D. Kivlichan, T. Menke, B. Peropadre, N. P. Sawaya, *et al.*, "Quantum chemistry in the age of quantum computing," Chemical reviews **119**, 10856–10915 (2019).
[5] P. W. Shor, "Algorithms for quantum computation: discrete logarithms and factoring," in *Proceedings 35th annual symposium on foundations of computer science* (Ieee, 1994) pp. 124–134.
[6] A. Y. Kitaev, "Quantum measurements and the abelian stabilizer problem," arXiv preprint quant-ph/9511026 (1995).
[7] A. Y. Kitaev, A. Shen, and M. N. Vyalyi, *Classical and quantum computation*, 47 (American Mathematical Soc., 2002).
[8] J. Preskill, "Quantum computing in the nisq era and beyond," Quantum **2**, 79 (2018).
[9] P. W. Shor, "Scheme for reducing decoherence in quantum computer memory," Phys. Rev. A **52**, R2493–R2496 (1995).
[10] A. G. Fowler, M. Mariantoni, J. M. Martinis, and A. N. Cleland, "Surface codes: Towards practical large-scale quantum computation," Physical Review A **86** (2012), 10.1103/physreva.86.032324.
[11] P. W. Shor, "Scheme for reducing decoherence in quantum computer memory," Physical review A **52**, R2493 (1995).
[12] A. M. Steane, "Simple quantum error-correcting codes," Physical Review A **54**, 4741 (1996).
[13] Y. Kim, M. Sevior, and M. Usman, "Magic state injection on ibm quantum processors above the distillation threshold," (2024), arXiv:2412.01446 [quant-ph].

[14]W. Kolos and L. Wolniewicz, "Improved theoretical ground-state energy of the hydrogen molecule," The Journal of chemical physics **49**, 404–410 (1968).
[15]J. T. Seeley, M. J. Richard, and P. J. Love, "The bravyi-kitaev transformation for quantum computation of electronic structure," The Journal of chemical physics **137** (2012).
[16]S. B. Bravyi and A. Y. Kitaev, "Fermionic quantum computation," Annals of Physics **298**, 210–226 (2002).
[17]I. Kassal, J. D. Whitfield, A. Perdomo-Ortiz, M.-H. Yung, and A. Aspuru-Guzik, "Simulating chemistry using quantum computers," Annual review of physical chemistry **62**, 185–207 (2011).
[18]R. Woolley and B. Sutcliffe, "Molecular structure and the born—oppenheimer approximation," Chemical Physics Letters **45**, 393–398 (1977).
[19]Y. Zhang, "Quantum computing simulation of the hydrogen molecule system with rigorous quantum circuit derivations," (2022).
[20]T. Helgaker, P. Jorgensen, and J. Olsen, *Molecular electronic-structure theory* (John Wiley & Sons, 2013).
[21]M. Suzuki, "Generalized trotter's formula and systematic approximants of exponential operators and inner derivations with applications to many-body problems," Communications in Mathematical Physics **51**, 183–190 (1976).
[22]C. Moler and C. Van Loan, "Nineteen dubious ways to compute the exponential of a matrix, twenty-five years later," SIAM review **45**, 3–49 (2003).
[23]K. M. Svore, D. P. DiVincenzo, and B. M. Terhal, "Noise threshold for a fault-tolerant two-dimensional lattice architecture," (2006), arXiv:quant-ph/0604090 [quant-ph].
[24]P. Aliferis, D. Gottesman, and J. Preskill, "Quantum accuracy threshold for concatenated distance-3 codes," (2005), arXiv:quant-ph/0504218 [quant-ph].
[25]B. Eastin and E. Knill, "Restrictions on transversal encoded quantum gate sets," Physical Review Letters **102** (2009), 10.1103/physrevlett.102.110502.
[26]D. Aharonov and M. Ben-Or, "Fault tolerant quantum computation with constant error," (1996), arXiv:quant-ph/9611025 [quant-ph].
[27]M. A. Nielsen and I. L. Chuang, *Quantum computation and quantum information*, Vol. 2 (Cambridge university press Cambridge, 2001).
[28]A. M. Steane, "Error correcting codes in quantum theory," Phys. Rev. Lett. **77**, 793–797 (1996).
[29]A. Mondal and K. K. Parhi, "Quantum circuits for stabilizer error correcting codes: A tutorial," IEEE Circuits and Systems Magazine **24**, 33–51 (2024).
[30]Y. Shee, P.-K. Tsai, C.-L. Hong, H.-C. Cheng, and H.-S. Goan, "Qubit-efficient encoding scheme for quantum simulations of electronic structure," Physical Review Research **4**, 023154 (2022).